The NSs protein encoded by the virulent strain of Rift Valley fever virus targets the expression of Abl2 and the actin cytoskeleton of the host affecting cell mobility, cell shape and cell-cell adhesion

Aline Bamia, Vasco Marcato, Magali Boissière, Zeyni Mansuroglu, Carole Tamietti, Mattea Romani, Dominique Simon, Guanfang Tian, Florence Niedergang, Jean-Jacques Panthier, et al.

The NSs protein encoded by the virulent strain of Rift Valley fever virus targets the expression of Abl2 and the actin cytoskeleton of the host affecting cell mobility, cell shape and cell-cell adhesion

Running title: RVFV NSs protein targets the host's actin cytoskeleton

Aline Bamia[1*], Vasco Marcato[1*], Magali Boissière[2], Zeyni Mansuroglu[1,3], Carole Tamietti[2], Mattea Romani[1], Dominique Simon[4], Guanfang Tian[1], Florence Niedergang[3], Jean-Jacques Panthier[4], Marie Flamand[2], Sylvie Souès[1,3] and Eliette Bonnefoy[1,3#]

[1]Université Paris Descartes, INSERM UMRS-1007 CICB-Paris, Paris, France ;

[2]Institut Pasteur, Unité de Recherche de Virologie Structurale, Paris, France;

[3]Université de Paris, Institut Cochin, INSERM, U1016, CNRS, UMR 8104, Paris, France;

[4]Institut Pasteur, Unité de Génétique Fonctionnelle de la Souris, Paris, France.

[*]Aline Bamia and Vasco Marcato equally contributed to this work. Author order was determined alphabetically.

abstract word count= 250

text word count = 7922

[#]corresponding author: eliette.bonnefoy@inserm.fr

Abstract

Rift Valley fever virus (RVFV) is a highly pathogenic zoonotic arbovirus endemic in many African countries and the Arabian Peninsula. Animal infections cause high rates of mortality and abortion among sheep, goats and cattle. In humans, an estimated 1-2% of RVFV infections result in severe disease (encephalitis, hepatitis, retinitis) with a high rate of lethality when associated to hemorrhagic fever. RVFV's NSs protein, which is RVFV's main factor of virulence, counteracts the host innate antiviral response favoring viral replication and spread. However, the mechanisms underlying RVFV-induced cytopathic effects and the role of NSs in these alterations remain for the most undeciphered. In this work we have analyzed the effects of NSs expression on actin cytoskeleton while conducting infections with the NSs expressing virulent (ZH548) and attenuated (MP12) strains of RVFV and the non-NSs expressing avirulent (ZH548ΔNSs) strain as well as after the ectopic expression of NSs. In macrophages, fibroblasts and hepatocytes NSs expression prevented the up-regulation of Abl2 (a major regulator of actin cytoskeleton) expression otherwise induced by avirulent infections and identified here as part of the antiviral response. The presence of NSs was also linked to and increased mobility of ZH548- as compared to ZH548ΔNSs-infected fibroblasts and to strong changes in cell morphology in non-migrating hepatocytes with reduction of lamellipodia, cell spreading and dissolution of adherens junctions reminiscent of ZH548-induced cytopathic effects observed *in vivo*. Finally, we show evidence of the presence of NSs within long actin-rich structures associated to NSs dissemination from NSs expressing towards non-NSs expressing cells.

Importance. Rift Valley fever virus (RVFV) is a dangerous human and animal pathogen that was ranked in 2018 by the World Health Organization among the eight pathogens of most concern likely to cause wide epidemics in the near future for which there is no, or insufficient, countermeasures. The interest of this work resides in the fact that it addresses the question of

48 the mechanisms underlying RVFV-induced cytopathic effects that participate in RVFV's
49 pathogenicity. We demonstrate here that RVFV targets cell adhesion and actin cytoskeleton at
50 the transcriptional and cellular level, affecting cell mobility and inducing cell shape collapse
51 alongside with distortion of cell-cell adhesion. All these effects are susceptible to participate
52 in RVFV-induced pathogenicity, facilitate virulent RVFV dissemination and thus constitute
53 interesting potential targets in future development of antiviral therapeutic strategies that in the
54 case of RVFV, as several other emerging arboviruses, are presently lacking.
55
56
57

Introduction

Rift Valley fever virus (RVFV) is a dangerous human and animal pathogen ranked in 2018 by the World Health Organization among the eight pathogens of most concern likely to cause wide epidemics in the near future for which there is no, or insufficient, countermeasures (https://www.who.int/blueprint/priority-diseases/en/). It is a mosquito-borne, zoonotic, phlebovirus endemic throughout many African countries and the Arabian Peninsula (1). Animal infections cause high rates of neonatal mortality and abortion mainly among sheep, goats and cattle. Human infections lead to a wide range of clinical manifestations from mild flue-like symptoms to severe illness such as encephalitis, retinitis and hepatitis, which can be fatal when associated to hemorrhagic fever. An estimated 1-2% of human infections result in severe disease often associated to high levels of mortality (1-3).

RVFV is an enveloped, segmented RNA virus of negative or ambisense polarity. It has a tripartite single-stranded RNA genome consisting of the large (L) and medium (M) segments of negative polarity and the small (S) segment of ambisense polarity. The L segment encodes the RNA-dependent RNA polymerase, the M segment encodes two glycoproteins as well as two non-structural NSm proteins and the S segment encodes the nucleoprotein N with a negative polarity and the nonstructural NSs protein with a positive polarity (2, 4, 5). The NSs protein that is produced shortly after infection (6) is not essential for the viral cycle but is considered as the main virulence factor of RVFV. Indeed, the virulent ZH548 strain that expresses NSs kills wild type mice whereas mutant viruses carrying a NSs-deletion, either natural (Clone 13) or recombinant (ZH548ΔNSs), are avirulent and non-pathogenic for mice (7, 8). NSs is characterized by its capacity to accumulate in the cell nucleus where it forms filament-like structures (9, 10) that include NSs itself as well as several cellular transcription factors and co-factors (11, 12). NSs has been found associated to specific cellular DNA sequences such as pericentromeric major satellite DNA sequences in

relation with chromosome cohesion defects (13) and the promoter region of the gene coding for interferon-beta (IFNβ), a cytokine that plays a major role in the innate antiviral response of the host, maintaining the IFNβ gene (*Ifnb1*) in a repressed state (12). Alongside with inhibiting the expression of *Ifnb1* (7, 12, 14), NSs also counteracts the cellular innate immune response by targeting kinase PKR for degradation (15). The inhibition of the host's innate antiviral response directly affects, facilitating, viral replication and propagation. However, the mechanisms, including the role of NSs, underlying the development of significant ultrastructural changes such as cell shrinkage, rounding and loss of cell junctions that have been observed *in vivo* in the liver after RVFV infection (16), potentially participating in RVFV's pathogenicity, remain for the most to be identified.

In previous work, we have performed a genome-wide analysis of the interactions between NSs and the host genome. For this, genome-wide chromatin immunoprecipitation (Chip) carried out using an anti-NSs antibody was combined with promoter sequence microarray hybridization (ChIP-on-chip). The DNA immunoprecipitated in these experiments was recovered from L929 murine fibroblastic cells either before or at different times post-infection (p.i.) with the pathogenic, NSs-expressing ZH548 strain of RVFV (17). Several cellular promoter regions were identified as significantly interacting with NSs and the establishment of NSs interactions with these regions was often linked to the deregulation of the expression of the corresponding genes. Among annotated NSs interacting genes were present not only genes regulating innate immunity and inflammation but also genes regulating cellular pathways potentially participating in RVFV's pathogenicity. The functional analysis of the genes associated to these NSs-interacting regions, identified cell adhesion as the biological process the most significantly enriched among cellular NSs-interacting genes (17).

In order to test the effect of RVFV infection and NSs protein in cell adhesion, we have compared in this work the effects of infections with the NSs expressing strains either virulent

ZH548 (ZH) or attenuated (MP12) and the non-expressing NSs avirulent ZH548ΔNSs (ΔNSs) strain of RVFV on actin cytoskeleton and cell-cell adhesion at the transcriptional and cellular level. We show here that the expression of the host's Abl2 protein, actin cytoskeleton organization and cell-cell adhesion were differently affected after infection by NSs-expressing and non-expressing strains of RVFV. Abl2 is a cytosolic protein encoded by the *Abl2* gene (also known as *Arg* for Abelson related gene) that is considered as a major regulator of actin cytoskeleton, regulating cell morphology and mobility as well as cell-cell and cell-matrix adhesion (18-23). Within its sequence, Abl2 contains a tyrosine kinase domain and two filamentous actin (F-actin) binding domains (20). Through its kinase domain Abl2 regulates Rho GTPases resulting in a negative regulation of focal adhesion and stress fiber formation, attenuating cell contractility and altering adhesion dynamics, that leads to the negative regulation of cell migration (18) and the positive regulation of adherens junction formation (21). Through its F-actin binding domains, Abl2 affects cell shape positively regulating lamellipodia and membrane ruffles (20, 22). In this work we have identified the up regulation of Abl2 expression as part of the cellular response meant to restrict virulence, which was counteracted by the NSs protein following either infection by the ZH and MP12 strains of RVFV or the ectopic expression of NSs.

ΔNSs infection induced the activation of Abl2 expression that was correlated to a diminution of cell migration. On the contrary, ZH infection prevented Abl2 up regulation in fibroblast, macrophages and hepatocytes subsequently hampering the ΔNSs-induced reduction of cell migration. Thus fibroblasts infected with virulent ZH strain migrated faster than fibroblasts infected with the avirulent ΔNSs strain. In the case of non-migrating hepatocytes, infection with ZH but not ΔNSs induced a strong collapse of cell shape and the distortion of cell-cell adhesion. Similar effects on Abl2 expression and cell structure were observed after infection with the NSs-expressing attenuated MP12 strain of RVFV as well as

following the ectopic expression of RVFV's NSs protein on hepatocytes where NSs was identified as the viral factor responsible for the inhibition of the up regulation of Abl2 expression, capable also to autonomously affect the host's actin cytoskeleton. Interestingly, NSs protein was found abundantly present within the cytoplasm of ZH- and MP12-infected hepatocytes as well as within long actin-rich structures connecting neighboring cells. While working with the attenuated MP12 strain at low multiplicity of infection, these NSs containing actin-rich structures were found associated to the dissemination of NSs from infected to non-infected cells.

We demonstrate here that infection with the virulent strain of RVFV targets cell adhesion and actin cytoskeleton at the transcriptional and cellular level, affecting cell mobility and inducing cell shape collapse alongside with distortion of adherens junctions. We propose that the up regulation of Abl2 expression is part of the host's strategy to restrict virulence and we discuss here how its counteraction by RVFV's NSs protein added to NSs effects on actin-cytoskeleton and cell-cell adhesion alongside with the presence of NSs within intercellular actin-rich structures could facilitate RVFV dissemination and pathogenicity.

Results

Avirulent and virulent strains of RVFV differently affected the expression of the gene coding for Abl2, a main regulator of actin cytoskeleton.

Infection with the virulent ZH548 (ZH) strain of RVFV is characterized by the presence of the non-structural NSs protein within the nucleus of infected cells, which is absent from cells infected with the avirulent ZH548ΔNSs (ΔNSs) strain lacking NSs (Fig.1A). While, as expected, the structural N protein encoded by RVFV was expressed in cells infected by ZH as well ΔNSs.

With the aim to investigate the effect of RVFV infection on the expression of genes regulating cell adhesion, the main biological function of the host represented among NSs interacting promoter regions (17), the expression profile of 12 out of the 96 NSs-interacting genes associated with cell adhesion was analyzed in this work by quantitative qPCR (Fig.1B). The expression rates of these 12 genes, chosen because described as expressed in many different cell types, were analyzed with respect to three reference genes, in three different cell lines (fibroblasts, hepatocytes, macrophages) under conditions of either non-infection (NI) or at two different times after infection with either the ZH or the ΔNSs strain of RVFV.

In Fig.1B are shown the ZH/ΔNSs expression ratios for the 12 genes tested. The expression of all genes excepting *Cdc42*, *Psen1* and *Pvrl1* displayed a minimum of 2 fold differences in at least one cell line with the expression of the *Abl2* gene being negatively affected in all the cell lines and at all the time points tested (Fig.1B). As compared to NI conditions, *Abl2* gene expression was enhanced after ΔNSs- but not ZH-infection in the three cell lines tested (Fig. 1C) with consistent results observed also at the protein level (Fig.1D and E). These results suggested a potential role for Abl2 in the innate antiviral response, as its

expression was induced after ΔNSs that induces the innate antiviral response whereas it was blocked after ZH infection that counteracts the innate antiviral response.

Abl2 behaves as a gene associated to the cellular innate antiviral response independent of interferon-beta signaling.

In order to consolidate the potential link between Abl2 expression and the innate antiviral response, Abl2 expression was further analyzed after infection of L929 cells (corresponding to the murine fibroblasts used in Fig.1) with the Newcastle Disease Virus (NDV). NDV is a *Paramyxoviridae* that, such as the ΔNSs strain of RVFV, is a good inducer of the innate antiviral response in murine cells (24, 25). The expression level of the *Abl2* gene was measured throughout the time course of infection by RT-qPCR alongside with the expression of genes related to the IFNβ response, a main actor of the innate antiviral response (26, 27), such as the *Ifnb1* gene coding for IFNβ and the *Oas1b* and *Irf7* genes corresponding to two well characterized Interferon β Stimulated Genes (ISGs) (Fig.2A).

NDV infection of L929 cells induced the expression not only of the *Ifnb1*, *Oas1b* and *Irf7* genes as expected, but also that of the *Abl2* gene (Fig.2A) as previously observed after ΔNSs infection (Fig.1C). Again, the effects observed at the transcriptional level were also observed at the protein level (Fig.2B and C). While the kinetics of expression of the ISGs *Oas1b* and *Irf7* were, as expected, delayed compared to that of the *Ifnb1* gene, the kinetics of the expression of the *Abl2* gene resembled more that of the *Ifnb1* gene suggesting that the virus-induced activation of the expression of *Abl2* would be independent of IFNβ. The role of IFNβ signaling on NDV-induced *Abl2* expression was tested using an anti-IFNAR antibody that, by blocking the IFNβ receptor IFNAR, antagonizes the IFNβ response, neutralizing the expression of ISGs (28). As expected, a dose-dependent inhibition of the expression of *Oas1b* and *Irf7* was observed in the presence of the anti-IFNAR antibody (Fig.2D). However, no

196 effect was detected on the expression of the *Abl2* gene under the same conditions indicating
197 that although *Abl2* behaved as a gene associated to the innate antiviral response, its expression
198 in the context of NDV infection appeared independent of IFNβ signaling.
199
200 **Activation of Abl2 expression in the context of ΔNSs but not ZH infection was correlated**
201 **with the negative regulation of cell migration.**
202 In order to investigate the potential implication of the opposite effects of ΔNSs and
203 ZH infection on Abl2 expression, we compared the effects of these two strains of RVFV on
204 cell migration that is negatively regulated by Abl2 (18, 19, 23).
205 Wound healing assays (scratch tests) were carried out on monolayers of confluent
206 L929 fibroblasts, which are fast migrating cells, either NI or infected by the ΔNSs or ZH
207 strains of RVFV. The coverage of the open (scratched) cell-free area by migrating fibroblasts
208 was assessed over time using bright-field imaging. The % of open, cell-free, area was
209 determined by an automated quantitative analysis using the TScratch software (29).
210 Wounding, which corresponded to T=0 h, was performed 24 h after plating the cells on glass
211 cover slips and immediately before infection. Cell counting performed at the beginning (T=0
212 h) and the end (T=20 h) of the assay indicated that confluent cells did not divide during the
213 time lapse of the experiment (data not shown).
214 Under these experimental conditions, NI L929 fibroblasts reached complete coverage
215 of the open area at 20 h after wounding (Fig.3A). TScratch analysis of the % of open area
216 showed that infection with the ΔNSs and ZH strains of RVFV differently affected cell
217 migration (Fig.3B). Infection with the ΔNSs strain significantly inhibited cell migration with
218 ΔNSs-infected cells displaying significantly higher % of open area than NI cells starting 15h
219 p.i. (Fig.3B). Infection with the ZH strain hampered the inhibitory effect of ΔNSs on cell
220 migration. ZH-infected cells migrated faster than ΔNSs-infected cells with ZH-infected cells

displaying significant lower % of open area than ΔNSs-infected cells starting 15 h p.i. (Fig.3B). The inhibitory effect of the ΔNSs strain of RVFV on cell migration was also observed after NDV infection with NDV-infected cells displaying significantly higher % of open area than NI cells starting 15 h p.i. (Fig.3C). Overall these results were in agreement with the role of Abl2 as a negative regulator of cell migration (18) since ΔNSs- and NDV-infected cells that expressed the highest amount of Abl2 corresponded to the slowest migrating cells displaying the highest % of open area.

In order to question the role of Abl2 on the capacity to slow down cell migration in the context of viral infection we used imatinib, which is an inhibitor of the Abl2 kinase activity that has been previously used to counteract Abl2-dependent inhibition of cell migration (30). The % of wound area under NI and NDV-infected conditions, in the presence or absence of imatinib, was measured 15 h after wounding with 100% corresponding to the open wound area under NI conditions in the absence of imatinib (Fig.3D). As previously observed, in the absence of imatinib, the % of open wound area was significantly higher after NDV infection than in NI cells (Fig.3D) in agreement with previous NDV-dependent reduction of cell migration. In the presence of imatinib, the capacity of NDV infection to negatively affect cell migration was significantly diminished (Fig.3D) indicative of a role for Abl2 kinase activity on NDV-induced inhibition of cell migration.

Virulent RVFV infection affected cell morphology and adherens junctions

While through its kinase activity Abl2 negatively regulates cell migration in link with the attenuation of cell contractility and focal adhesion dynamics (18), it positively regulates cell spreading through its two F-actin binding domains promoting the formation of actin-rich structures at the lamellipodia (22, 31, 32). The impact of ΔNSs and ZH infection on cell morphology was analyzed independently of cell migration by fluorescence and confocal

246 microscopy using phalloidin as a marker of F-actin. Experiments were carried out on
247 hepatocytes (AML12 cell line) that constitute one of the main cell types targeted during
248 RVFV infection with liver damage in association with hemorrhagic fever being the most
249 frequent cause of death in humans (1-3). Under our experimental conditions AML12 cells did
250 not display migratory capacity neither before nor after infection with either ΔNSs or ZH
251 strains of RVFV (data not shown) thus allowing the analysis of cell structure independently of
252 cell migration. Despite the propensity of AML12 cells to adhere to each other, isolated cells
253 were identified that were used here to analyze effects on cell structure (Fig.4A-D). Important
254 changes in cell morphology were consistently observed after infection with the ZH strain with
255 respect to NI and ΔNSs-infected cells for which representative images are shown in Fig.4A.
256 While NI and ΔNSs-infected cells displayed significant cell spreading, ZH-infected cells
257 displayed a reduction of cell spreading, lamellipodia and membrane ruffles, and a
258 disorganization of actin fibers visible from 8h p.i. (Fig.4A). Also, long F-actin-rich structures
259 (indicated by an arrow in Fig.4A) were often seen present among isolated ZH-infected cells.
260 ImageJ software was used to quantify changes in cell shape and area based on phalloidin
261 staining of NI, ΔNSs- and ZH-infected cells. Original images were transformed into binary
262 images (Fig.4B) and the outlines of the binary images were used to measure cell area (Fig.4C)
263 and circularity (Fig.4D). Even though not statistically significant, a trend towards an
264 enhancement of cell area was observed 18h p.i. under conditions of ΔNSs infection with
265 respect to NI and ZH infection (Fig.4C) this being in agreement with the up-regulation of
266 Abl2 expression observed in ΔNSs-infected with respect to NI and ZH-infected cells
267 (Fig.1C). In addition, a significant increase in cell circularity was observed after ZH infection
268 at 18h p.i. with respect not only to ΔNSs infected cells but also NI cells (Fig.4D).
269 AML12 cells have a strong propensity to establish cell-cell contacts forming adherens
270 junctions that contain β-catenin. Abl2 has been described to positively regulate β-catenin

stability (333) and maintain adherens junctions (19, 21). In agreement with distinct effects on Abl2 expression, infections with ΔNSs and ZH strains differently affected the stability of β-catenin containing cell junctions (Fig. 4E). At late times after infection (18h p.i.), ΔNSs-infected cells appeared to sustain β-catenin containing cell junctions, while a systematic dissolution of β-catenin containing cell junctions was observed after infection with ZH (Fig.4E). At earlier (8 h) times p.i., disruption of β-catenin containing adherens junctions was evidenced among ZH-infected cells with accumulated NSs (Fig.4F). Dissolution of adherens junctions among ZH-infected AML12 cells resulted in loosening of cell-to-cell contact, visible after F-actin labeling in ZH-infected NSs-expressing with respect to NI cells (Fig. 4G) with the strongest effect observed among the cells displaying the highest amount of NSs (indicated by white arrows in Fig.4G).

Interestingly, while analyzing the distribution of Abl2 in ZH-infected cells with respect to NSs protein we observed a co-localization of Abl2 with NSs that started to be visible at 8h p.i. (indicated by arrows in Fig.4H) and was clearly enhanced 24 h p.i. (Fig.4H). Even though not visible among all NSs expressing cells, Abl2 co-localization with NSs appeared associated to dissolution of adherens junctions (24 h p.i.) (Fig.4H).

The NSs-expressing MP12 strain of RVFV affected Abl2 expression and cell morphology similarly to the ZH strain

In order to further confirm the main role of NSs in targeting the actin-cytoskeleton of the host at the transcriptional and cellular level, we carried out infections with RVFV's MP12 strain that even though attenuated by several mutations in its S, M and L segments still encodes for a functional NSs protein (34, 35). The NSs protein encoded by the MP12 strain formed filamentous structures in the nuclei of AML12-infected cells (Fig. 5A) similarly to the ZH-encoded NSs protein (Fig.4). The NSs-dependent inhibition of IFNβ gene expression is a

major trait observed after ZH infection (7, 8, 12, 23). Comparison of IFNβ expression in NI, ΔNSs-, ZH- and MP12-infected AML12 cells indicated that, as in the case of ZH infection, MP12 infection strongly inhibited the expression of the IFNβ gene otherwise induced by ΔNSs infection (Fig.5B). Alongside with measuring IFNβ expression, we also measured the level of Abl2 mRNA in NI, ΔNSs-, ZH- and MP12-infected cells (Fig.5C). The significant ΔNSs-dependent induction of Abl2 expression previously observed in AML12 cells (Fig.1C), and reproduced here, was significantly hampered not only after infection with the ZH strain in agreement with our previous observations but also after MP12 infection (Fig.5C). Consistently, as in ZH-infected cells, the expression of NSs in MP12-infected cells was correlated with a strong alteration of cell shape and spreading (Fig. 5D) and with a loosening of adherens junctions (Fig.5E) for which representative images are shown here. Results obtained after MP12 infection at low multiplicity of infection (MOI), confirmed the correlation between NSs expression and disruption of β-catenin rich adherens junctions (as indicated by a white arrow in Fig.5E) as compared to non-NSs expressing cells. Overall, the results obtained, which are in agreement with previously reported functional similarity between MP12 and ZH encoded NSs proteins (34), confirmed the capacity of NSs protein to affect actin cytoskeleton hampering the up-regulation of Abl2 expression and affecting cell shape and cell-to-cell adhesion.

ZH and MP12 encoded NSs proteins are found present within long actin-rich structures in association with intercellular NSs dissemination

AML12 cells infected with MP12 displayed not only nuclear but also a cytoplasmic distribution of NSs. In Fig.5E, the cytoplasmic staining of NSs extended more than 30 μms away from the nucleus of the corresponding NSs-expressing cell, reaching towards non-NSs expressing cells through weakened adherens junctions (as indicated by a grey arrow in

321 Fig.5E). Cytoplasmic NSs protein was also detected in non-infected cells (indicated by an
322 arrow in Fig.5F), suggesting a dispersion from neighboring infected cells expressing N and
323 NSs favored by disrupted adherens junctions.

324 The presence of cytoplasmic NSs aggregates was a consistent trait observed not only
325 among MP12-infected cells but also among ZH-infected cells that persisted throughout
326 infection and remained visible 18h p.i. (Fig.6A). Among ZH-infected cells, NSs protein was
327 very often visible within F-actin-rich extensions as indicated by white arrows in
328 representative Fig.6A. Occasionally, these actin-rich extensions extended over a long distance
329 interconnecting cells more than 100 μm apart (Fig. 6B), terminating in an apparent delivery
330 process of the NSs protein into the cell body of a neighboring cell (Fig.6B, insets) suggesting
331 a cell-to-cell spreading of NSs.

332 In order to further investigate the capacity of NSs to disseminate from NSs-expressing
333 to non-NSs expressing cells, we carried out infections with the attenuated strain of MP12 at a
334 low MOI. Viral replication and the % of NSs positive cells were jointly analyzed throughout
335 infection. Viral replication was determined by measuring the relative expression of N and
336 NSs RNAs by RT-qPCR and the percentage of NSs expressing cells was analyzed after
337 fluorescent labeling of cells with Hoechst and anti-NSs antibodies. In order to carry out a
338 random analysis of NSs+ cells, cells were counted according to Hoechst staining before
339 further analyze for NSs staining. Measurements were done throughout two independent
340 infections with each infection carried out with a different batch of MP12 RVFV (Figs.6C and
341 D). Even though differences in the levels of N and NSs expression and in the percentage of
342 NSs expressing cells were observed between the two infections, the values evolved according
343 to the same pattern (Figs.6C and D). MP12 RVFV stopped replicating 24 p.i. with the relative
344 expression of N and NSs RNAs remaining constant (infection#1) or slightly diminishing
345 (infection#2) between 24 and 48h p.i. (Fig.6C). The percentage of NSs positive cells was

346 proportional to the amount of N and NSs RNA between the two infections as well as between
347 8 and 24 h p.i. for each infections. However, notwithstanding a stop in the increase of N and
348 NSs RNA expression, the percentage of NSs positive cells continued to increase between 24
349 and 48 h p.i. in both infections (Fig.6D). MP12 infection has been shown to induce cell cycle
350 arrest (36), similarly to what we have previously shown in the case of ZH infection (13), thus
351 the increase of NSs+ positive cells observed between 24 and 48 h p.i. suggested the existence
352 of a cell-cycle independent mechanism of dissemination of NSs from NSs-expressing towards
353 non-NSs expressing cells.

354 The distribution of NSs+ cells was further analyzed among microscope field of views
355 specifically selected for NSs staining. In Fig.6E are shown representative images of fields of
356 views selected for NSs staining at 8, 24 and 48 h p.i. in the case of infection#1. At 8 h p.i. no
357 more than one NSs+ cell was observed within a field, at 24 h p.i. clusters of NSs+ cells
358 appeared (indicated by a white arrow in Fig.6E) with an average of 11.6 % of NSs+ cells
359 present *per* field. The clustered distribution of NSs+ cells was further enhanced at 48h p.i. so
360 that an average of 58.4 % of NSs+ cells were present *per* field selected for NSs staining
361 (Fig.6E). Yet, when counting NSs+ cells in a random selection of field views, only an average
362 of 3.25 % of NSs+ cells at 24h, with several fields displaying none, rising to 7.6 % *per*
363 random field at 48h p.i. was determined (Fig.6D).

364 A cytoplasmic spreading of NSs more than 30 μm away from the cell's nucleus was
365 again observed 24 h p.i. (indicated by a grey arrow in Fig.6E). Also, a gradient-like
366 distribution of NSs was observed 48 h p.i. (indicated by a triangle in Fig.6E), suggesting a
367 from cell to cell spreading of NSs. In order to further confirm the spreading of NSs from
368 NSs+ towards non-NSs expressing cells, we looked for NSs dissemination events under
369 conditions for which only a small percentage NSs+ cell were detected in a field view, such as
370 was the case during infection#1 of AML12 cells by MP12 at low MOI 24h p.i.. Under these

conditions, NSs dissemination events were indeed identified such as the one shown in Fig.6F where an infected, NSs-expressing cell (indicated by an arrow) bridges two non-infected, non-NSs expressing cells through long actin-rich NSs-containing structures that ended up in a NSs delivery process (Fig.6F). Even though the N protein of RVFV was also visible within actin rich extensions, only NSs was delivered to non-infected cells as observed in previous Fig.5F.

RVFV's N protein was consistently found present within long actin-rich structures in the context of ZH infection but to a lesser extent following MP12 infection at low MOI (Fig.6G). Since NSs protein was similarly present within long actin rich extensions in the context of ZH and low MOI MP12 infections, the differential staining observed here for RVFV's N protein in long actin rich extensions, for the most not co-localizing with NSs, suggested that the N protein of RVFV was not necessary for NSs to be present within these structures.

The ectopic expression of NSs protein mimics ZH infection

The presence of the non-structural NSs protein within intercellular actin-rich protrusions raised the question of the potential capacity of NSs to convey virulent phenotypes autonomously, independently of other viral factors.

The capacity of the ectopically expressed NSs protein to induce ZH-like phenotypes was tested by transfecting non-infected AML12 cells with either a plasmid carrying the cDNA coding for NSs (pCI-NSs) or the empty vector (pCI). Twenty-four hours after transfection, the expression of NSs RNA was detected in AML12 cells transfected with pCI-NSs and not in pCI-transfected cells (Fig.7A). The expression of NSs RNA was calculated here with respect to three reference genes (*Ppib*, *Utp6c* and *Hprt1*) for which the corresponding expression rates did not vary after transfection with either pCI-NSs or pCI.

Indicative that at least 24 h after its expression, NSs did not significantly affected the transcriptional capacity of AML12 cells. This lack of effect on the transcriptional capacity of the host observed here 24 h after NSs expression is in agreement with our previous observations in ZH-infected L929 cells (17) and with more recently reported results in MP12-infected HEK293 cells (37). Notwithstanding variations observed from one transfection assay to another, 10-30 % of the pCI-NSs transfected cells were identified at the single cell level as expressing NSs protein by immunofluorescence using anti-NSs antibody. In these cells, the ectopically expressed NSs protein formed nuclear filamentous structures (Fig.7B) resembling those observed after infection with the virulent ZH strain of RVFV. However, compared to ZH- and MP12-infected AML12 cells, the ectopically expressed NSs protein displayed an exclusively nuclear distribution with no NSs detected outside the nucleus, suggesting that a viral component other than NSs could be required to induce a cytoplasmic NSs distribution in AML12 cells.

The effect of the ectopically expressed NSs protein on actin cytoskeleton and cell morphology was analyzed by fluorescence and confocal microscopy using phalloidin to label F-actin alongside with anti-NSs antibodies. Cells transfected with the empty vector (Fig. 7C, pCI) displayed a morphology and an actin cytoskeleton organization similar to that of non-transfected, non-infected AML12 cells (Fig. 4A). Among AML12 cells transfected with pCI-NSs (Fig. 7C, pCI-NSs), those cells that ectopically expressed NSs (indicated by arrowheads in Fig.7C) displayed a strong reduction of cell spreading and a disorganization of F-actin fibers similarly to ZH- and MP12-infected AML12 cells (Figs. 4A and 5D). Therefore the non-structural NSs protein alone, in the absence of any other RVFV component, was able to induce changes in cell morphology similar to those induced by the virulent ZH strain. The effect of the ectopically expressed NSs protein on the expression of the *Abl2* gene was also analyzed. No significant changes in *Abl2* gene expression were observed among cells

transfected with pCI-NSs as compared to pCI (Fig.7D). This was similar to the lack of effect of ZH and MP12 infection on the level of Abl2 expression displayed by NI AML12 cells (Figs.1C and 5C respectively) and further confirmed the absence of effect of NSs expression on the host transcriptional capacity. However, the ectopic expression of NSs was capable to significantly inhibit the expression of the *Abl2* gene induced after infection with NDV (Fig.7D), similarly to the previously observed capacity of ZH and MP12 infection to prevent the increase of *Abl2* gene expression otherwise induced by ΔNSs (Figs.1C and 5C respectively), further confirming the capacity of NSs protein to mimic ZH-induced effects independently of any other protein encoded by RVFV.

The capacity of the ectopically expressed NSs protein to mimic the effects of ZH infection on ΔNSs-induced cellular gene expression was further analyzed for genes participating in the IFNβ response and the coagulation cascade whose expressions have been previously reported to be affected after ZH with respect to ΔNSs infection (17, 24). As shown in Fig. 7D, the ectopic expression of NSs in AML12 cells significantly inhibited the NDV-induced activation of the expression of the genes related to the IFNβ response (such as the *Ifnb1* gene coding for IFNβ and the two ISGs *Irf7* and *Oas1b*) while it activated the expression of the *F10* gene coding for coagulation factor F10, as it was previously observed after infection with the ZH strain with respect to ΔNSs-infected cells (17).

Overall these results demonstrated that the NSs protein encoded by RVFV had the capacity to autonomously induce phenotypes similar to those observed after infection with the pathogenic virulent ZH strain of RVFV, raising the question of the potential deleterious effects that could be conveyed by the intercellular spreading of NSs protein.

Discussion

We show here evidence that the viral NSs protein, which is the major factor of virulence of RVFV, affects the actin cytoskeleton of the host at the transcriptional and cellular level. At the transcriptional level, NSs expression counteracted the up-regulation of Abl2 expression, a major regulator of actin cytoskeleton that in this work was found associated to the cellular response to a viral infection. At the cellular level, the presence of NSs was associated to strong changes in cell morphology that were reminiscent of the effects on cell and tissue structures observed after ZH infection *in vivo* (16).

Besides a major role for NSs on cell structure and actin cytoskeleton organization, we describe here for the first time an effect of RVFV's NSs-expressing ZH strain on cell mobility with ZH- migrating faster than ΔNSs-infected cells. In the case of influenza virus infection, restriction of cell mobility was found to be highly protective (38). Similarly, we hypothesize that the reduction of cell mobility induced here after avirulent ΔNSs infection in correlation with an up-regulation of Abl2 expression would be necessary to limit viral dissemination by migrating innate immune cells such as macrophages, dendritic cells, neutrophils and microglia that are infected by RVFV *in vitro* and/or *in vivo* (39, 40). Hampering reduction of cell mobility, as observed here following virulent ZH infection, could favor virulence and pathogenicity. In agreement with this hypothesis, a recent work has shown a major role for the migration into the central nervous of innate immune cells carrying a viral antigen in lethal RVFV encephalitis in Lewis rats (40).

Abl2 has been shown to negatively regulate cell mobility in link with the negative regulation of cell contractility and focal adhesion dynamics resulting from Abl2 regulation of the activity of Rho GTPases (18-20). Also, Abl2 positively regulates cell-cell adhesion (in link with its negative effect on cell contractility and the stabilization of β-catenin) (19, 21, 33) and cell spreading in link with its capacity to directly interact with F-actin (22, 31, 32). The

effects on cell mobility observed after ΔNSs infection with respect to NI and ZH-infected cells were indeed those expected for an up-regulation of Abl2 expression. Also in agreement with ΔNSs-induced up-regulation of Abl2 expression, a trend towards cell spreading and consolidation of adherens junctions was observed in ΔNSs- with respect to non-infected cells. If the effects of ΔNSs infection on cell morphology remained weak, it is probably because NI AML12 cells expressed Abl2, displayed substantial cell spreading and consistent formation of β-catenin rich adherens junctions before ΔNSs infection, independently of an up-regulation of Abl2 expression. Therefore, no more than limited effects on AML12 cell morphology with no further significant enhancement of cell spreading and cell-cell adhesion, are expected following ΔNS-induced up-regulation of Abl2.

In the case of either ZH and MP12 infection or ectopic expression of NSs, the morphological changes induced in link with NSs expression resembled those expected for Abl2 deficient cells. However, these changes were not always correlated with differences in Abl2 expression. In fact, strong morphological differences were observed not only between ΔNSs- and ZH- or MP12-infected cells but also between ZH- and non-infected cells while both displayed similar levels of Abl2 expression. However, it is plausible that the association of Abl2 with NSs filaments highlighted in this work could impact Abl2's capacity to interact with the actin cytoskeleton and thus participate in the establishment of the NSs-dependent morphological changes resembling Abl2 deficient phenotypes.

Nonetheless, even though NSs-dependent effects on cell mobility and cell morphology resembled those expected for Abl2 deficient phenotypes, the direct link between the targeting of Abl2 by NSs and NSs-dependent effects on actin cytoskeleton shown in this work remains presently to be demonstrated.

The presence of long intercellular actin-rich NSs-containing structures, associated to the dissemination of NSs protein, was another feature of ZH- and MP12-infected AML12

493 cells. These structures are reminiscent of the actin-rich intercellular connections that have
494 been described to facilitate virus spreading to neighboring cells, as in the case of influenza A
495 virus (41), HIV-1 (42) or lymphocytic choriomeningitis virus (LCMV) (43). Cell-to-cell
496 transmission of the LCMV through actin-rich intercellular structures was facilitated by virus-
497 induced enhanced cell migration (43), an interesting feature with respect to the capacity of ZH
498 infection to hamper negative regulation of cell mobility. Actin-rich intercellular structures
499 have also been described to facilitate the dissemination of prion and prion-like proteins (44,
500 45). *In vivo,* only a very small fraction of the host cells are primary infected cells and the
501 efficiency of the host's antiviral response largely depends on the paracrine IFNβ signaling
502 triggered by the small number of cells initially infected (46). NSs was proven here to be able
503 to affect the host's IFNβ response alone, independently of any other viral compound.
504 Therefore, the dissemination of NSs from NSs-expressing to non-NSs expressing cells that we
505 have shown here to occur at a low MOI between nneighboring cells through disrupted
506 adherens junctions or long actin rich structures, could have strong negative effects on the
507 capacity of the host to stop viral dissemination *in vivo*.

508 The presence of NSs within actin-rich extensions and NSs dissemination was observed
509 here in ZH- and MP12-infected AML12 cells that displayed a dual nuclear/cytoplasmic
510 distribution of NSs but was not observed in cells ectopically expressing NSs that displayed
511 only a nuclear NSs distribution. A recent work by Li *et al*. (10) has demonstrated an
512 important role *in vivo* for the dual nuclear and cytoplasmic distribution of NSs in RVFV's
513 virulence and pathogenicity. In order to question the possible role of the subcellular
514 distribution of NSs protein in regulating intercellular NSs spreading, it would be necessary to
515 analyze the effect of the different rRVFVs established by Li *et al*. (10) on NSs dissemination.
516 Li et al. (10) have described cytoplasmic versus nuclear distribution of NSs in relation with
517 specific regions of NSs. This suggests a role for NSs structure and/or NSs interaction with

518 another protein in the regulation of the nuclear/cytoplasmic distribution of NSs. The absence
519 of cytoplasmic NSs among cells ectopically expressing NSs suggested a role for another viral
520 component in this process.

521 At the transcriptional level, NSs altered not only the expression of Abl2 but also that
522 of other genes involved in cell adhesion. For instance, we showed here (Fig.1) that, compared
523 to ΔNSs, ZH infection negatively impacted *Lgals3bp* gene expression that codes for an
524 extracellular matrix protein promoting integrin-mediated cell-matrix and cell-cell adhesion
525 (47, 48). Also, while analyzing alterations in the host transcriptome following infection with
526 the ZH strain of RVFV with respect to non-infected cells, Pinkham et al. (49) identified the
527 Interleukin-linked kinase (ILK) pathway as one of the main host's pathways altered after
528 infection. ILK connects the extracellular matrix to actin cytoskeleton by interacting with the
529 cytoplasmic domain of β integrins regulating several functions related to actin cytoskeleton
530 organization. Interestingly, the cytoplasmic tail of β3 integrin has been shown to directly
531 interacts with Abl2 (22) thus connecting Abl2 with ILK signaling, further establishing cell
532 adhesion as a main biological processes targeted by RVFV.

533 Overall we have shown here that infection with the virulent ZH strain of RVFV
534 prevented the up-regulation of the expression of Abl2, counteracted ΔNSs-induced inhibition
535 of cell migration, affected cell shape and induced the dissolution of adherens junctions. These
536 effects were shown here to be dependent on the expression of NSs that itself was shown to be
537 present within long actin-rich structures involved in the dissemination of NSs to neighboring,
538 non-NSs expressing cells. These NSs-dependent effects on the host's actin cytoskeleton are
539 susceptible to participate in RVFV-induced pathogenicity by facilitating virulent RVFV
540 dissemination and thus could constitute interesting potential targets in future development of
541 antiviral therapeutic strategies that in the case of RVFV, as several other emerging
542 arboviruses, are presently lacking.
543

Materials and Methods

Virus and cells

Stocks of RVFV ZH548, ZH548ΔNSs and MP12 were produced under BSL3 conditions by infecting Vero cells at m.o.i. of 10^{-3} and harvesting the medium at 72 hr p.i. Cell lines were cultured at 37 °C under 5% CO_2 in medium supplemented with 10 μg/mL penicillin/streptomycin (Gibco, Thermo Scientific) and 10% (v/v) fetal calf serum (FCS, Gibco). Murine fibroblastic L929 (ATCC) cells were grown in MEM medium (Gibco). Murine hepatocyte, alpha mouse liver 12, AML12 cells (ATCC ref. CRL-2254) were cultured in DMEM-F12 medium (Gibco) supplemented with 0.005 mg/mL insulin, 0.005 mg/mL transferrin, 5 ng/mL selenium (Sigma) and 40 ng/mL dexamethasone (Gibco, Thermo Scientific). Non-infected cells (NI) correspond to mock-infected cells that were treated as infected cells except that no virus was added. When indicated, antibody directed against the mouse IFN a/b receptor 1 (clone MAR1-5A3 from BD Biosceinces n°561183) was added directly to the media 15 h before infection and kept in the media during the entire time of infection. All infections were carried out at an MOI=5 unless otherwise indicated.

Antibodies

Primary antibodies used for immunofluorescence and/or Western blot were mouse anti-NSs and rabbit anti-N polyclonal antibodies raised against the entire NSs or N protein of RVFV respectively (9); anti-β-catenin monoclonal antibody (BD Transduction laboratories Cat#610154); anti-Abl2 (anti-Arg ref 07-262) from Merck Millipore and anti-GAPDH (ref 3781) from ProSci. Secondary antibodies used for immunofluorescence were Alexa 488 fluor-conjugated chicken anti-mouse from Invitrogen (A21200) and Alexa 555 fluor-conjugated donkey anti-rabbit from Invitrogen (A31572). Secondary antibodies used for

Western blot were ECL Mouse IgG, HRP-linked whole Ab (NA931) and ECL Rabbit IgG, HRP-linked whole Ab (NA934) from GE Healthecare Life Sciences.

Immunofluorescence.

Cells grown in 6-well plates on coverslips were fixed with 3.7 % formaldehyde in phosphate-buffered saline (PBS) for 15 min and permeabilized with 1 % Triton X-100 in PBS for 20 min. The cells were incubated for 1 h at room temperature with the corresponding primary antibodies diluted in PBS-5% bovine serum albumin. After washing with PBS the cells were next incubated for 45 min at room temperature with the corresponding secondary antibodies or phalloïdin-FITC (Sigma P5282).

Image analysis and quantification.

Samples were analyzed at room temperature by confocal laser scanning microscopy using a AxioImager Z2 (Zeiss LSM710 confocal system). This system is equipped with a 63× lens, 1.4-numerical-aperture oil immersion lens (Plan Neofluor). For oil immersion microscopy, we used oil with refractive index of 1.518 (Zeiss). Images were captured in the z-axis corresponding to the optical axis of the microscope at 0.37 µm intervals with the z-axis going through the image planes. LSM Zen imaging software was used for image capture. The images were analyzed by the LSM5 Image browser or Image J software. All images are representative of a minimum of two independent infections for all conditions described in this work. The Analyze Particle Plugin of Image J was use to analyze and quantify cell shape and area.

Cell transfection.

Plasmid pCI-NSs used for heterologous NSs protein expression contains the cDNA sequence of NSs from ZH548 RVFV strain (50). Twenty-four hours before transfection, AML12 cells were plated in 6 well plates at a density of 2 10^5 cells per well. Mix A containing 2 μg of plasmid diluted in 50 μl of low fetal bovine serum OptiMEM media was added to mix B containing 5 μl of Lipofectamine 2000 (ref 11668-027, Invitrogen) diluted in 195 μl of OptiMEM and incubated at room temperature for 20 min before being dispensed into the well. Transfected cells were further incubated as previously described for 24 h before treatment.

Scratch wound healing assay.

Murine fibroblast L929 cells were plated on coverslips in 6-well plates at a density of 600.000 cells/well and cultured as previously described for 24 h to reach full confluence before scratch. Cell monolayers were scratched with a P10 pipette tip, incubated in fresh MEM medium supplemented with 10% FBS and treated as indicated in Fig.3. After treatment cells were fixed in 3.7 % formaldehyde for 20 min. Images were collected at indicated times under a wild field microscope and quantitatively analyzed using the T-Scratch software (30).

RT-qPCR

Total RNA was extracted using Tri Reagent (Sigma) according to the manufacturer's protocol. 1 µg of total RNA was reversely transcribed using High Capacity cDNA Reverse Transcription Kit (Applied Biosystems) according to the manufacturers' recommendations using Random Primers. qPCR was performed using SYBR Green (Thermo Scientific) reagents: 95°C 15 minutes, then 40 cycles at 95°C 15 seconds, 60°C 30 seconds, 72°C 15 seconds, followed by a dissociation step. Relative quantification of mRNA expression was calculated using the $\Delta\Delta C_T$ method using three reference genes among Ppib, Hprt1, Utp6c and

Rplp0. For fold changes lower than 1 (translating a repression of the gene's expression), values were set such that a (½) fold change corresponds to -2, a (¼) corresponds to -4 and so on. Sequences (5'-3') of primers used for RT-qPCR analysis were as follows= *Abl2* F: GAGCCACCGTTTTACATTGTGA and R: CTCGCCCACTAGGCAGTTC; *Cdc42* F: CTTCTTCGGTTCTGGAGGCT and R: GGGATCTGAAGGCTGTCAAG; *Fblim1* F: TAGCCGTGAGTGAGGAAGTG and R: CAGAGAGTGAGGCATTGGTCT; *Hprt1* F: TCCTCCTCAGACCGCTTTT and R: CCTGGTTCATCATCGCTAATC; *Ifnb1* F: ATGAACAACAGGTGGATCCTCC and R: AGGAGCTCCTGACATTTCCGAA; *Irf7* F: CAGCGAGTGCTGTTTGGAGAC and R: AAGTTCGTACACCTTATGCGG; *Lgals3bp* F: TGCTGGTTCCAGGGACTCAA and R: CCACCGGCCTCTGTAGAAGA; *Lpp* F: GCAACCAAGAAGTCCGCAAC and R: GCCGTAGTATAGGAGGCTGGA; *N* protein of RVFV F: AAGGCAAAGCAACTGTGGAG and R: CAGTGACAGGAAGCCACTCA; *NSs* protein of RVFV F: GCACCTCCACCAGCGAAGCC and R: CCAGTGAGGGTTCTCCAAGAGGC; *Oas1b* F: GAGGTGCCGACGGAGGT and R: TCCAGATGAAGTCTTCCCAAAG; *Pkp2* F: GCCGAGTGTGGCTACATCC and R: CTGCTGGTTCGGTGAAGGTT; *Ppib* F: GGAGATGGCACAGGAGGAAA and R: CCGTAGTGCTTCAGTTTGAAGTTCT; *Psen1* F: ATACCTGCACCTTTGTCCTACT and R: GCTCAGGGTTGTCAAGTCTCT; *Ptprf* F: CTGCTCTCGTGATGCTTGGTT and R: ATCCACGTAATTCGAGGCTTG; *Pvrl1* F: GACTCCATGTATGGCTTCATCG and R: CACTCGTTTCTCGTAGGGAGG; *Rplp0* F: CACTGGTCTAGGACCCGAGAAG and R: GGTGCCTCTGGAGATTTTCGk; *Thbs1* F: GGGGAGATAACGGTGTGTTTG and R: CGGGGATCAGGTTGGCATT; *Utp6c* F: TTTCGGTTGAGTTTTTCAGGA and R: CCCTCAGGTTTACCATCTTGC; *Vezt* F: AACCCCGAACACTTGGGATG and R: GAAGGCTCGGCTATTGGCTG; *Vtn* F: CCCCTGAGGCCCTTTTTCATA and R: CAAAGCTCGTCACACTGACA.

641

642 **Western blot**

643 Total protein extracts were prepared from cells grown in 6-well plates in 250 μl/well
644 of RIPA lysis buffer to containing phosphatase inhibitor PhoSTOP (Roche, 04 906 856 001)
645 and protease inhibitor (Roche, 04 693 132 001). After centrifugation at 14 000 rpm for 10 min
646 at 4°C, lysates were heated in Laemmli buffer and loaded in NuPAGE 4-12 % sodium
647 dodecyl sulfate-polyacrylamide precast gels (Life Technologie). Loaded proteins were
648 transferred on PolyVinyliDene diFluoride (PVDF) membrane. Membranes were incubated
649 overnight at 4°C with primaty antibodies, washed with TBS-T (Tris Base Sodium Tween 0.1
650 %) and incubated with the corresponding secondary antibodies for 1 h at room temperature.
651 Imager ImageQuant LAS4000 was used for chemiluminescent protein detection. Relative
652 quantification of proteins was carried out using Image J software.

653

Declarations

Acknowledgements

Agence Nationale de la Recherche (ANR) provided funding to Eliette Bonnefoy, Marie Flamand and Jean-Jacques Panthier under grant number ANR-11-BSV3-007. The DIM-Malinf project from Région Ile-de-France provided funding to Vasco Marcato.

References

1. Wright D, Kortekaas J, Bowden TA, Warimwe GM. Rift Valley fever: biology and epidemiology. J Gen Virol. 2019; 100(8):1187-1199.
2. Ikegami T. Molecular biology and genetic diversity of Rift Valley fever virus. Antiviral Res. 2012; 95(3):293-310.
3. Pepin M, Bouloy M, Bird BH, Kemp A, Paweska J. Rift Valley fever virus (Bunyaviridae:Phlebovirus): an update on pathogenesis, molecular epidemiology, vectors, diagnostics and prevention. Vet Res. 2010; 41(6):61.
4. Elliott RM, Brennan B. Emerging phleboviruses. Curr Opin Virol. 2014; 5:50-7.
5. Kreher F, Tamietti C, Gommet C, Guillemot L, Ermonval M, Failloux AB, Panthier JJ, Bouloy M, Flamand M. The Rift Valley fever accessory proteins NSm and P78/NSm-GN are distinct determinants of virus propagation in vertebrate and invertebrate hosts. Emerg Microbes Infect. 2014; 3(10):e71.
6. Ikegami T, Won S, Peters CJ, Makino S. Rift Valley fever virus NSs mRNA is transcribed from an incoming anti-viral-sense S RNA segment. J Virol. 2005; 79(18):12106-11.
7. Bouloy M, Janzen C, Vialat P, Khun H, Pavlovic J, Huerre M, Haller O. Genetic evidence for an interferon-antagonistic function of rift valley fever virus nonstructural protein NSs. J Virol. 2001; 75(3):1371-7.
8. Billecocq A, Gauliard N, Le May N, Elliott RM, Flick R, Bouloy M. RNA polymerase I-mediated expression of viral RNA for the rescue of infectious virulent and avirulent Rift Valley fever viruses. Virology. 2008; 378(2):377-84.
9. Yadani FZ, Kohl A, Préhaud C, Billecocq A, Bouloy M. The carboxy-terminal acidic domain of Rift Valley Fever virus NSs protein is essential for the formation of

filamentous structures but not for the nuclear localization of the protein. J Virol. 1999; 73(6):5018-25.

10. Li **S,** Zhu X, Guan Z, Huang W, Zhang Y, Kortekaas J, Lozach PY, Peng K. NSs Filament Formation Is Important but Not Sufficient for RVFV Virulence In Vivo.Viruses. 2019; 11(9).

11. Le May N, Dubaele S, Proietti De Santis L, Billecocq A, Bouloy M, Egly JM. TFIIH transcription factor, a target for the Rift Valley hemorrhagic fever virus. Cell. 2004; 116(4):541-50.

12. Le May N, Mansuroglu Z, Léger P, Josse T, Blot G, Billecocq A, Flick R, Jacob Y, Bonnefoy E, Bouloy M. A SAP30 complex inhibits IFN-beta expression in Rift Valley fever virus infected cells. PLoS Pathog. 2008; 4(1):e13.

13. Mansuroglu Z, Josse T, Gilleron J, Billecocq A, Leger P, Bouloy M, Bonnefoy E. Nonstructural NSs protein of rift valley fever virus interacts with pericentromeric DNA sequences of the host cell, inducing chromosome cohesion and segregation defects. J Virol. 2010; 84(2):928-39.

14. Wuerth JD, Weber F. Phleboviruses and the Type I Interferon Response. Viruses. 2016; 8(6).

15. Habjan M, Pichlmair A, Elliott RM, Overby AK, Glatter T, Gstaiger M, Superti-Furga G, Unger H, Weber F. NSs protein of rift valley fever virus induces the specific degradation of the double-stranded RNA-dependent protein kinase. J Virol. 2009; 83(9):4365-75.

16. Reed C, Steele KE, Honko A, Shamblin J, Hensley LE, Smith DR. Ultrastructural study of Rift Valley fever virus in the mouse model. Virology. 2012 ; 431:58-70.

17. Benferhat R, Josse T, Albaud B, Gentien D, Mansuroglu Z, Marcato V, Souès S, Le Bonniec B, Bouloy M, Bonnefoy E. Large-scale chromatin immunoprecipitation with promoter sequence microarray analysis of the interaction of the NSs protein of Rift Valley fever virus with regulatory DNA regions of the host genome. J Virol. 2012; 86(20):11333-44.

18. Peacock JG, Miller AL, Bradley WD, Rodriguez OC, Webb DJ, Koleske AJ. The Abl-related gene tyrosine kinase acts through p190RhoGAP to inhibit actomyosin contractility and regulate focal adhesion dynamics upon adhesion to fibronectin. Mol Biol Cell. 2007; 18(10):3860-72.

19. Bradley WD, Koleske AJ. Regulation of cell migration and morphogenesis by Abl-family kinases: emerging mechanisms and physiological contexts. J Cell Sci. 2009; 122(Pt 19):3441-54.

20. Khatri A, Wang J, Pendergast AM. Multifunctional Abl kinases in health and disease. J Cell Sci. 2016; 129(1):9-16.

21. Zandy NL, Playford M, Pendergast AM. Abl tyrosine kinases regulate cell-cell adhesion through Rho GTPases. Proc Natl Acad Sci U S A. 2007; 104(45):17686-91.

22. Zhang K, Lyu W, Yu J, Koleske AJ. Abl2 is recruited to ventral actin waves through cytoskeletal interactions to promote lamellipodium extension. Mol Biol Cell. 2018; 29(23):2863-2873.

23. Torsello B, De Marco S, Bombelli S, Chisci E, Cassina V, Corti R, Bernasconi D, Giovannoni R, Bianchi C, Perego RA. The 1ALCTL and 1BLCTL isoforms of Arg/Abl2 induce fibroblast activation and extra cellular matrix remodelling differently. Biol Open. 2019; 8(3).

24. Marcato V, Luron L, Laqueuvre LM, Simon D, Mansuroglu Z, Flamand M, Panthier JJ, Souès S, Massaad C, Bonnefoy E. β-Catenin Upregulates the Constitutive and

731 Virus-Induced Transcriptional Capacity of the Interferon Beta Promoter through T-
732 Cell Factor Binding Sites. Mol Cell Biol. 2016; 36(1):13-29.
733 25. Higashi Y. Changes of chromatin conformation around mouse interferon-beta gene
734 associated with induction of interféron synthesis. Nucleic Acids Res. 1985;
735 13(14):5157-72.
736 26. Schneider WM, Chevillotte MD, Rice CM. Interferon-stimulated genes: a complex
737 web of host defenses. Annu Rev Immunol. 2014;32:513-45.
738 27. Hubel P, Urban C, Bergant V, Schneider WM, Knauer B, Stukalov A, Scaturro P,
739 Mann A, Brunotte L, Hoffmann HH, Schoggins JW, Schwemmle M, Mann M, Rice
740 CM, Pichlmair A. A protein-interaction network of interferon-stimulated genes
741 extends the innate immune system landscape. Nat Immunol. 2019; 20(4):493-502.
742 28. Sheehan KC, Lai KS, Dunn GP, Bruce AT, Diamond MS, Heutel JD, Dungo-Arthur
743 C, Carrero JA, White JM, Hertzog PJ, Schreiber RD. Blocking monoclonal antibodies
744 specific for mouse IFN-alpha/beta receptor subunit 1 (IFNAR-1) from mice
745 immunized by in vivo hydrodynamic transfection. J Interferon Cytokine Res. 2006;
746 26(11):804-19.
747 29. Gebäck T, Schulz MM, Koumoutsakos P, Detmar M. TScratch: a novel and simple
748 software tool for automated analysis of monolayer wound healing assays.
749 Biotechniques. 2009; 46(4):265-74.

30. Procaccia V, Nakayama H, Shimizu A, Klagsbrun M. Gleevec/imatinib, an ABL2 kinase inhibitor, protects tumor and endothelial cells from semaphorin-induced cytoskeleton collapse and loss of cell motility. Biochem Biophys Res Commun. 2014; 448(2):134-8.

31. Wang Y, Miller AL, Mooseker MS, Koleske AJ. The Abl-related gene (Arg) nonreceptor tyrosine kinase uses two F-actin-binding domains to bundle F-actin. Proc Natl Acad Sci U S A. 2001; 98(26):14865-70.

32. Miller AL, Wang Y, Mooseker MS, Koleske AJ. The Abl-related gene (Arg) requires its F-actin-microtubule cross-linking activity to regulate lamellipodial dynamics during fibroblast adhesion. J Cell Biol. 2004; 165(3):407-19.

33. Gu JJ, Rouse C, Xu X, Wang J, Onaitis MW, Pendergast AM. Inactivation of ABL kinases suppresses non-small cell lung cancer metastasis. JCI Insight. 2016; 1(21):e89647.

34. Kalveram B, Lihoradova O, Indran SV, Ikegami T. Using reverse genetics to manipulate the NSs gene of the Rift Valley fever virus MP-12 strain to improve vaccine safety and efficacy. J Vis Exp. 2011; (57):e3400.

35. Ikegami T, Hill TE, Smith JK, Zhang L, Juelich TL, Gong B, Slack OA, Ly HJ, Lokugamage N, Freiberg AN. Rift Valley Fever Virus MP-12 Vaccine Is Fully Attenuated by a Combination of Partial Attenuations in the S, M, and L Segments. J Virol. 2015; (14):7262-76.

36. Baer A**,** Austin D, Narayanan A, Popova T, Kainulainen M, Bailey C, Kashanchi F, Weber F, Kehn-Hall K. Induction of DNA damage signaling upon Rift Valley fever virus infection results in cell cycle arrest and increased viral replication. J Biol Chem. 2012; 287(10):7399-410.

774 37. Havranek KE, White LA, Lanchy JM, Lodmell JS. Transcriptome profiling in Rift
775 Valley fever virus infected cells reveals modified transcriptional and alternative
776 splicing programs. PLoS One. 2019; 14(5):e0217497.
777 38. Jennings RT, Strengert M, Hayes P, El-Benna J, Brakebusch C, Kubica M, Knaus UG.
778 RhoA determines disease progression by controlling neutrophil motility and restricting
779 hyperresponsiveness. Blood. 2014;123(23):3635-45.
780 39. Gommet C, Billecocq A, Jouvion G, Hasan M, Zaverucha do Valle T, Guillemot L,
781 Blanchet C, van Rooijen N, Montagutelli X, Bouloy M, Panthier JJ. Tissue tropism
782 and target cells of NSs-deleted rift valley fever virus in live immunodeficient mice.
783 PLoS Negl Trop Dis. 2011;5(12):e1421.
784 40. Albe JR, Boyles DA, Walters AW, Kujawa MR, McMillen CM, Reed DS, Hartman
785 AL. Neutrophil and macrophage influx into the central nervous system are
786 inflammatory components of lethal Rift Valley fever encephalitis in rats. PLoS
787 Pathog. 2019;15(6):e1007833.
788 41. Roberts KL, Manicassamy B, Lamb RA. Influenza A virus uses intercellular
789 connections to spread to neighboring cells. J Virol. 2015;89(3):1537-49.
790 42. Bracq L, Xie M, Benichou S, Bouchet J. Mechanisms for Cell-to-Cell Transmission of
791 HIV-1. Front Immunol. 2018;9:260.
792 43. Labudová M, Čiampor F, Pastoreková S, Pastorek J. Cell-to-cell transmission of
793 lymphocytic choriomeningitis virus MX strain during persistent infection and its
794 influence on cell migration. Acta Virol. 2018;62(4):424-434.
795 44. Gousset K, Schiff E, Langevin C, Marijanovic Z, Caputo A, Browman DT, Chenouard
796 N, de Chaumont F, Martino A, Enninga J, Olivo-Marin JC, Männel D, Zurzolo C.
797 Prions hijack tunnelling nanotubes for intercellular spread. Nat Cell Biol.
798 2009;11(3):328-36.

45. Victoria GS, Zurzolo C. The spread of prion-like proteins by lysosomes and tunneling nanotubes: Implications for neurodegenerative diseases. J Cell Biol. 2017;216(9):2633-2644.

46. Patil S, Fribourg M, Ge Y, Batish M, Tyagi S, Hayot F, Sealfon SC. Single-cell analysis shows that paracrine signaling by first responder cells shapes the interferon-β response to viral infection. Sci Signal. 2015; 8(363):ra16.

47. Loimaranta V, Hepojoki J, Laaksoaho O, Pulliainen AT. Galectin-3-binding protein: A multitask glycoprotein with innate immunity functions in viral and bacterial infections. J Leukoc Biol. 2018;104(4):777-786.

48. Hepojoki J, Strandin T, Hetzel U, Sironen T, Klingström J, Sane J, Mäkelä S, Mustonen J, Meri S, Lundkvist A, Vapalahti O, Lankinen H, Vaheri A. Acute hantavirus infection induces galectin-3-binding protein. J Gen Virol. 2014;95(Pt 11):2356-64.

49. Pinkham C, Dahal B, de la Fuente CL, Bracci N, Beitzel B, Lindquist M, Garrison A, Schmaljohn C, Palacios G, Narayanan A, Campbell CE, Kehn-Hall K. Alterations in the host transcriptome in vitro following Rift Valley fever virus infection. Sci Rep. 2017;7(1):14385.

50. Billecocq A, Spiegel M, Vialat P, Kohl A, Weber F, Bouloy M, Haller O. NSs protein of Rift Valley fever virus blocks interferon production by inhibiting host gene transcription. J Virol. 2004;78(18):9798-806.

Figure Legends

Figure 1. Infection with RVFV affects the expression of genes related to cell adhesion including Abl2 expression. (**A**) Murine L929 fibroblasts either non-infected (NI) or infected with the virulent ZH548 (ZH) or the avirulent ZH548ΔNSs (ΔNSs) strains of RVFV were labeled 15 h p.i. using a DNA intercalating agent to visualize the nucleus (Hoechst, in blue), an antibody directed against the structural N protein of RVFV (N, in red) or an antibody directed against the non-structural NSs protein of RVFV (NSs, in green). (**B**, **C**) The expression of 12 genes associated with cell adhesion, previously identified to interact with the NSs protein of RVFV (17), was measured in macrophages (RAW cell line), hepatocytes (AML12 cell line) and fibroblasts (L929 cell line) either non-infected (NI) or at the indicated times after infection with ZH or ΔNSs strains. Purified RNAs were analyzed by RT-qPCR using Biomark with primers specific for each gene of interest. Relative quantification of mRNA expression was calculated with respect to three reference genes corresponding to *Hmbs*, *Ppib* and *Hprt1* in the case of RAW cells; *Hprt1*, *Ppib*, and *Rplp0* in the case of AML12 cells; *Ppib*, *Rplp0* and *Utp6c* in the case of L929 cells. In (**B**) the fold change in ZH-infected cells was calculated with respect to ΔNSs-infected cells. In (**C**) fold induction was calculated with respect to non(mock)-infected (NI) cells. Results correspond to the average of n (independent experiments)=3 in the case of AML12 and L929 cells for all conditions tested (except L929 ZH 16h for which n=2) and n=2 in the case of RAW cells for all conditions tested. Data are means ± s.d. One-way ANOVA Tukey's multiple comparison test. In (**B**), the expression level of certain genes could not be tested since the corresponding mRNA remained not detectable (ND). (**D**, **E**) Abl2 protein level was analyzed by Western blot in extracts from L929 cells non-infected (NI) or infected by the ΔNSs or ZH strains of RVFV. (**E**) Quantification using ImageJ of n (independent experiments)=3 in the case of ZH and ΔNSs 15 and 20 h p.i. and n=6 for NI 15 and 20 h. Data are means ± s.d. One-way ANOVA test

with Bonferroni correction. P-value <0.0001 (****), <0.001 (***), < 0.01 (**) and <0.05 (*); ns= not significant. Images correspond to a single confocal section. Bar=10 μm.

Figure 2. *Abl2* behaves as a gene of the cellular innate antiviral response independent of interferon-beta signaling. (**A**) The expression of genes associated to the IFNβ response, coding for IFNβ and for two ISGs (IRF7 and OAS1B), alongside with the gene coding for Abl2, was measured by RT-qPCR in L929 cells either non-infected (NI) or at different times after NDV infection. Relative expressions were determined with respect to three reference genes (*Utp6c*, *Ppib*, *Hprt1*) and fold inductions were calculated with respect to non-infected (NI) cells. Results correspond to the average of n (independent experiments)=3 for all conditions tested. Data are means ± s.d. Statistical analysis was carried out only for Abl2 gene expression using one-way ANOVA test with Dunnett correction with each NDV-infected condition compared to non-infected conditions. (**B**, **C**) Abl2 protein level was analyzed by Western blot in extracts from L929 cells non-infected (NI) or infected by NDV. (**C**) Quantification using ImageJ with n (independent experiments)=3 for NDV 8, 20 and 24 h p.i. and n=10 for NI. Data are means ± s.d. One-way ANOVA test with Dunnett correction and each NDV-infected condition compared to non-infected condition. (**D**) The expression of genes associated to the IFNβ response, coding for IFNβ and for two ISGs (IRF7 and OAS1B), alongside with the gene coding for Abl2, was measured by RT-qPCR in L929 cells collected 6 h p.i. with NDV, either not-treated or treated with increasing amounts of anti-IFNAR antibody. Relative expressions were determined with respect to three reference genes (*Utp6c*, *Ppib*, *Hprt1*) and fold inductions were calculated with respect to non-infected (NI) cells considered as 100%. Results correspond to the average of n (independent experiments)=4 for 0 μg; n=2 for 0.5 μg; n=3 for 1.5 and 5 μg of anti-IFNAR antibody. Data are means ± s.d. One-way ANOVA test with Bonferroni correction for each gene separately. P-value <0.001 (***), < 0.01 (**) and <0.05 (*).

Figure 3. Infection with ΔNSs or NDV reduced cell migration. (**A**) Representative bright-field images of a monolayer of confluent non-infected (NI) L929 cells taken at different times after introducing a scratch wound with a pipette tip. Images are shown before (original images) and after automated analysis by TScratch program. Percentage of open areas as determined by the TScratch program are indicated with 100% corresponding to the area of the entire image. (**B**, **C**, **D**) Scratch-wound closure of L929 cells was monitored over time in non-infected (NI) cells and after infection with ΔNSs or ZH (**B**) or NDV (**C**) or NDV 15h p.i. in presence or absence of imatinib (**D**). Wound closure is expressed as the % of remaining open area uncovered by cells as determined by the TScratch program with 100% corresponding in (**B**, **C**) to the scratch area of non-infected (NI) cells at time point 0 h and in (**D**) to the scratch area of non-infected cells at 15h in the absence of Imatinib. (**B**) For each condition (NI, ΔNSs and ZH), results correspond to the average of n (number of images analyzed)=18 (from 3 independent experiments) for 0, 8, 15 and 20 h; n=12 (from 2 independent experiments) for 10h. (**C**) For each condition (NI, NDV), results correspond to the average of n (number of images analyzed)=12 (from 2 independent experiments) for 0, 8, 15, 20 and 24 h. (**D**) Results correspond to the average of n (number of images analyzed)=9 (from 3 independent experiments). Data are means ± s.d. One-way ANOVA test with Bonferroni correction for each time point separately (**B**), for all samples (**D**) and Student's t-test in (**C**). P-value <0.0001 (****), <0.001 (***), < 0.01 (**) and <0.05 (*).

Figure 4. Infection with the virulent ZH but not the avirulent ΔNSs strain affects cell morphology and adherens junctions. Murine hepatocytes (AML12 cell line) either non-infected (NI) or infected with the avirulent ΔNSs or the virulent ZH strains of RVFV were labeled 8 h (**A**, **B**, **F** and **H**) and 18 h (**E**, **G** and **H**) p.i. using a DNA intercalating agent to visualize the nucleus (Hoechst, in blue), phalloidin to visualize filamentous actin (F-actin in green or grey in **A**, **B**, **G** and **H**), an anti-NSs antibody (NSs, in red), an anti-beta-catenin

antibody (b-cat in green in **E** and **F**) and an anti-Abl2 (Abl2 in green in **H**). White arrows indicate long F-actin-rich extensions in **A**, dissolution of adherens junctions in **F** and **G** and co-localization of Abl2 with NSs in **H**. (**B**) The analyze particle function of ImageJ software was used to transform the images into binary images and determine the cell outlines. (**C**, **D**) Main parameters such as the cell area and perimeter were determined and cell shape was analyzed by calculating the circularity= 4π x (area/perimeter^2). Results, from a minimum of 2 independent experiments for each condition, correspond to the average of n (number of cells analyzed)=70 for NI; n=11 for ΔNSs 8 h p.i.; n=18 for ΔNSs 18 h p.i. ; n=48 for ZH 8 h p.i.; n=21 for ZH 18 h p.i.. Data are means ± s.d. One-way ANOVA test with Dunnett correction with ΔNSs and ZH compared to NI and ΔNSs compared to ZH. P-value <0.05 (*). Images correspond to single confocal sections. Bar=10 μm.

Figure 5. Infection with the NSs-expressing MP12 of RVFV affects Abl2 expression and cell morphology. Murine AML12 hepatocytes infected with the MP12 strain of RVFV were labeled 8 h (**D**) and 24 h (**A**, **E**, **F**) p.i. using a DNA intercalating agent to visualize the nucleus (Hoechst, in grey or blue), antibodies directed against the non-structural NSs (in red) or the N (in green) proteins of RVFV and phalloidin to visualize filamentous actin (F-actin in green or grey). In **E** and **F** MP12 infection was carried out at a MOI=0.01. (**B**, **C**) The expression of the genes coding for IFNβ (**B**) and Abl2 (**C**) was measured by RT-qPCR in AML12 cells either non-infected (NI) or at the indicated times after infection with ΔNSs, ZH or MP12 strains. Relative expressions were determined with respect to *Rplp0* as reference gene and fold inductions were calculated with respect to non-infected (NI) cells. Results correspond to the average of n (independent experiments)=2. Data are means ± s.d. One-way ANOVA Tukey's multiple comparison test. (**E**) Grey arrow indicates NSs dissemination and white arrow indicates dissolution of adherens junctions. (**F**) White arrow indicates NSs

dissemination. P-value <0.05 (*). In **E and** F images correspond to single confocal sections. Bar=10 μm.

Figure. 6. ZH and MP12 encoded NSs proteins are found present within long actin-rich structures in association with intercellular dissemination. Murine hepatocytes (AML12 cell line) infected with the NSs-expressing ZH and MP12 strains of RVFV at an MOI= 0.01 in the case of MP12 were labeled 8 h (**B**, **E** and **G**), 18 h (**A**), 24 h (**E** and **F**) and 48 h (**E**) p.i. using a DNA intercalating agent to visualize the nucleus (Hoechst in grey or blue in **E**, **F** and **G**), phalloidin to visualize filamentous actin (F-actin in green or grey in **A**, **B** and **F**), an anti-NSs antibody (NSs, in red) and an anti-N antibody (N in green in **F** and **G**). White arrows indicate NSs-containing actin-rich structures in **A**, NSs dissemination in **E** and infected, NSs-expressing cells in **F**. White triangle indicates a gradient staining of NSs in **E**. (**C**) The expression N and NSs RNAs was measured by RT-qPCR in AML12 cells either non-infected (NI) or at the indicated times after infection with MP12 at an MOI= 0.01. Relative expressions were determined with respect to *Rplp0*. (**D**) The percentage of cells displaying NSs labeling was randomly determined at indicated times following MP12 infection at MOI= 0.01. In **A**, **B**, **F** and **G** images correspond to single confocal sections. Bar=10 μm.

Figure 7. The ectopic expression of NSs protein affects cell morphology and gene expression mimicking ZH infection. AML12 cells were transfected with a plasmid encoding the NSs protein of RVFV (pCI-NSs) or with the empty vector (pCI). Twenty-four hours after transfection, the presence of NSs mRNA was quantified by RT-qPCR (**A**) and the presence of NSs protein was analyzed by fluorescence (**B**) using an anti-NSs antibody (NSs, in green) and a DNA intercalating agent to visualize the nucleus (Hoechst, in blue). (**C**) Cell shape was analyzed by fluorescence using phalloidin to visualize filamentous actin (F-actin, in red) and a DNA intercalating agent to visualize the nucleus (Hoechst, in blue). (**D**) Twenty four hours

946 after transfection with plasmids pCI or pCI-NSs, transfected cells were either non-infected
947 (NI) or infected with NDV. Four hours after infection, RNA was collected and the expression
948 level of RNA coding for NSs, Abl2, IFN, Irf7, Oas1b and F10 was measured by RT-qPCR.
949 (**A**, **D**) Relative expressions were calculated with respect to three reference genes (*Ppib*,
950 *Utp6c*, *Hprt1*). In the case of the *Abl2*, *Ifnb1*, *Irf7* and *Oas1b* genes, the % of expression was
951 determined with respect to pCI+NDV conditions considered as 100%. (**A**, **D**) Results
952 correspond to an average of n (independent experiments)=3 except for the *Ifnb1* and *Oas1b*
953 genes for which n=4. Data are means ± s.d. (**D**) Student's t-test. P-value <0.001 (***), < 0.01
954 (**) and <0.05 (*). Images correspond to single confocal sections. Bar= 10 μm.
955

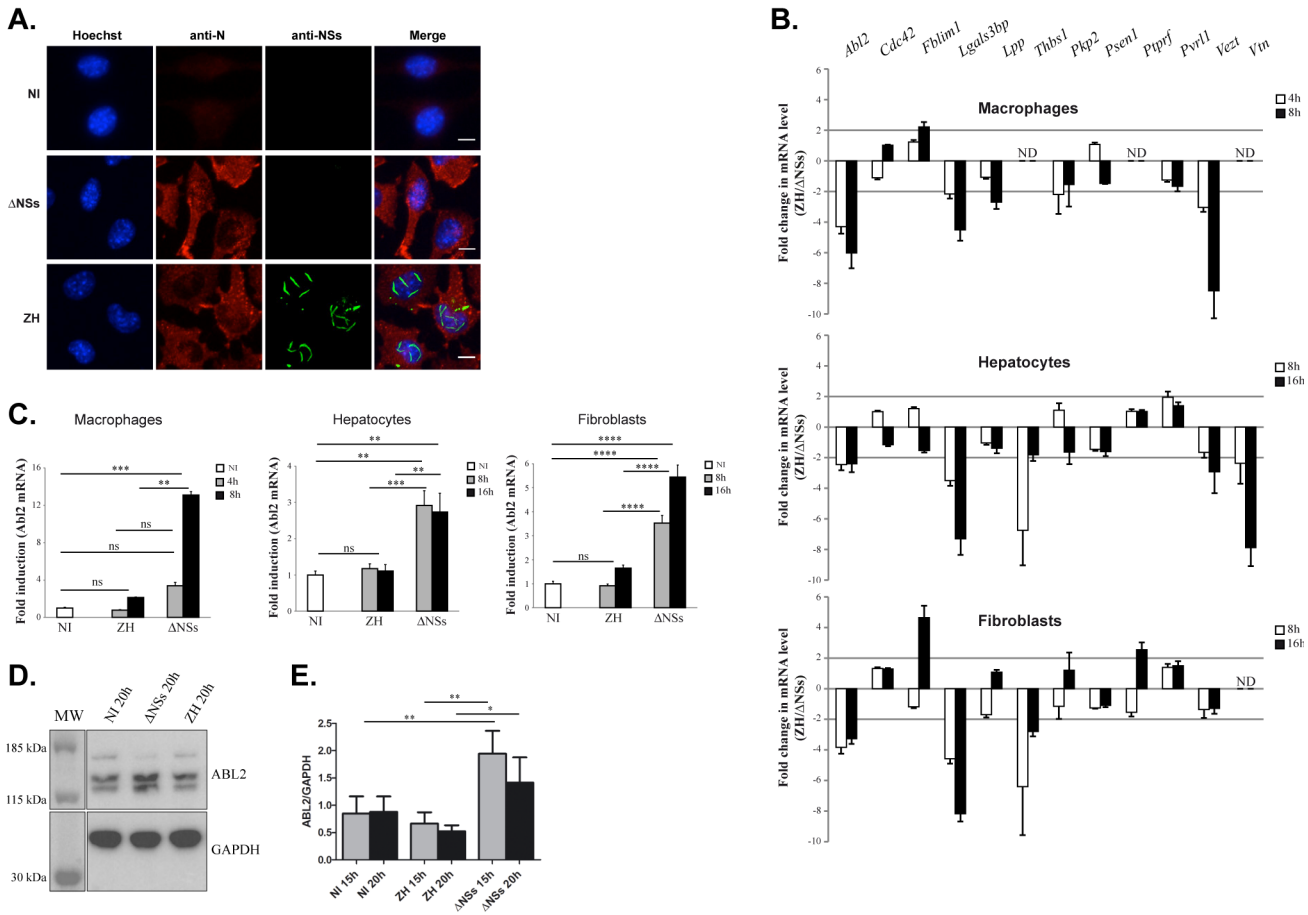
A.
Hoechst
anti-N
anti-NSs
Merge
NI
ΔNSs
ZH
B.
Abl2
Cdc42
Fblim1
Lgals3bp
Lpp
Thbs1
Pkp2
Psen1
Ptprf
Pvrl1
Vezt
Vtn
Macrophages
Hepatocytes
Fibroblasts
Fold change in mRNA level (ZH/ΔNSs)
ND
4h
8h
16h
C.
Macrophages
Hepatocytes
Fibroblasts
Fold induction (Abl2 mRNA)
NI
ZH
ΔNSs
ns
D.
MW
NI 20h
ΔNSs 20h
ZH 20h
185 kDa
115 kDa
30 kDa
ABL2
GAPDH
E.
ABL2/GAPDH
NI 15h
NI 20h
ZH 15h
ZH 20h
ΔNSs 15h
ΔNSs 20h

Figure 1

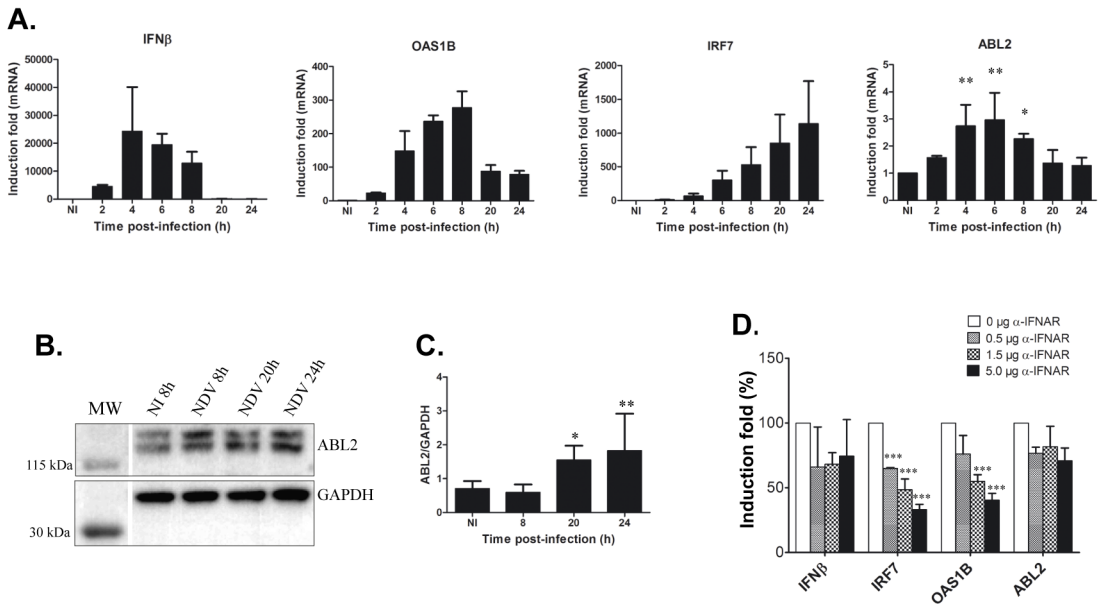
A.
IFNβ
OAS1B
IRF7
ABL2
Induction fold (mRNA)
Time post-infection (h)
NI
2
4
6
8
20
24
B.
MW
NI 8h
NDV 8h
NDV 20h
NDV 24h
115 kDa
30 kDa
ABL2
GAPDH
C.
ABL2/GAPDH
Time post-infection (h)
D.
0 µg α-IFNAR
0.5 µg α-IFNAR
1.5 µg α-IFNAR
5.0 µg α-IFNAR
Induction fold (%)
IFNβ
IRF7
OAS1B
ABL2

Figure 2

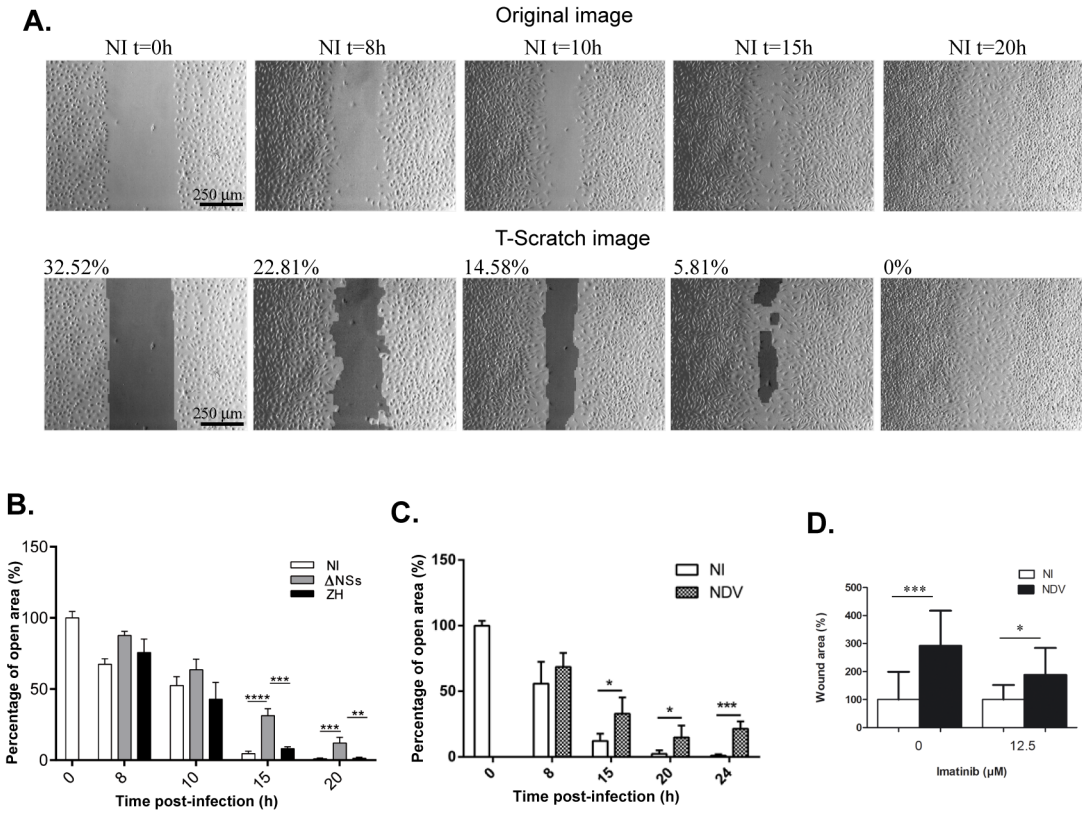
A.
Original image
NI t=0h
NI t=8h
NI t=10h
NI t=15h
NI t=20h
250 μm
T-Scratch image
32.52%
22.81%
14.58%
5.81%
0%
250 μm
B.
Percentage of open area (%)
NI
ΔNSs
ZH
Time post-infection (h)
C.
Percentage of open area (%)
NI
NDV
Time post-infection (h)
D.
Wound area (%)
NI
NDV
Imatinib (μM)

Figure 3

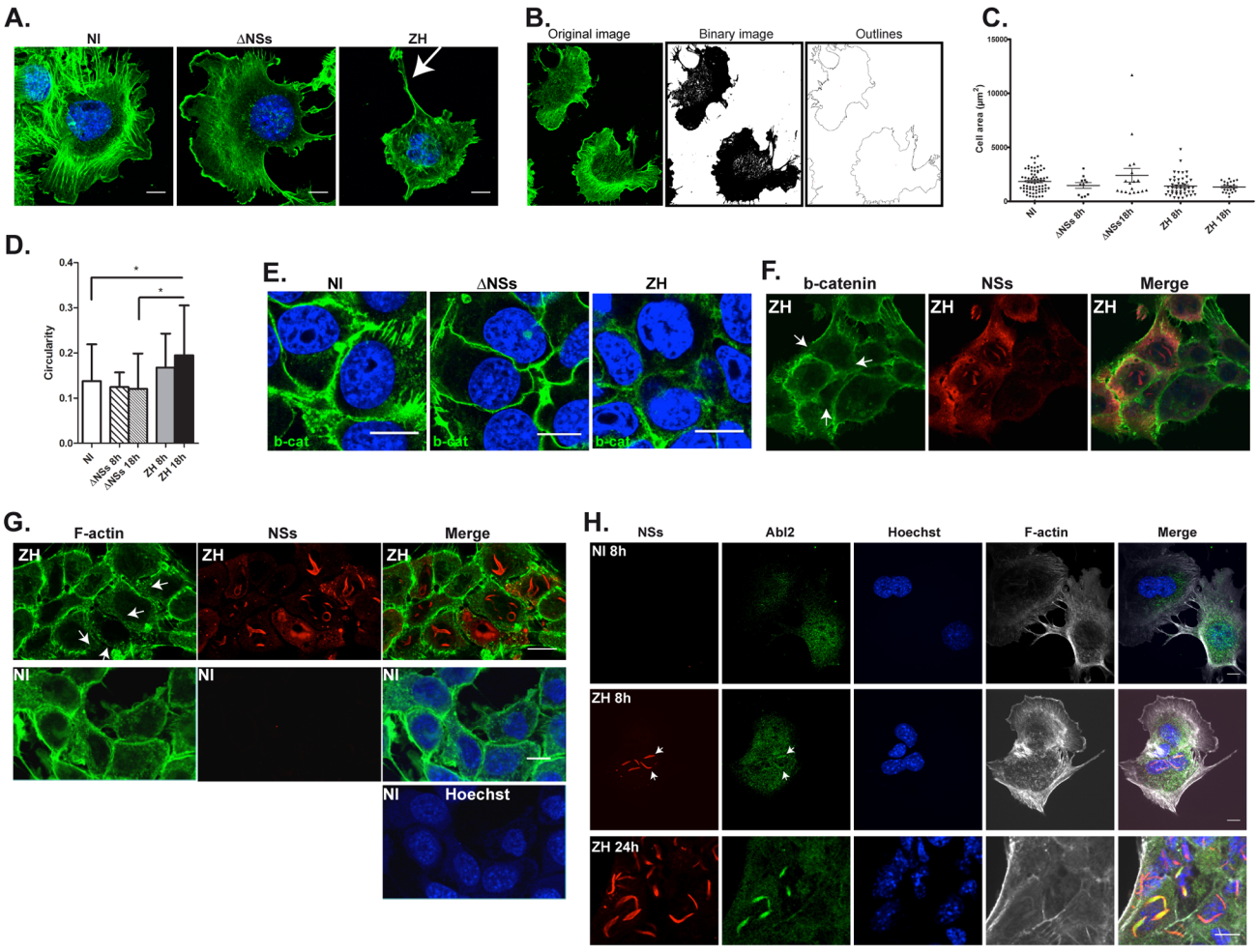
A.
NI
ΔNSs
ZH
B.
Original image
Binary image
Outlines
C.
Cell area (μm²)
15000
10000
5000
0
NI
ΔNSs 8h
ΔNSs18h
ZH 8h
ZH 18h
D.
Circularity
0.4
0.3
0.2
0.1
0.0
*
*
NI
ΔNSs 8h
ΔNSs 18h
ZH 8h
ZH 18h
E.
NI
ΔNSs
ZH
b-cat
b-cat
b-cat
F.
b-catenin
NSs
Merge
ZH
ZH
ZH
G.
F-actin
NSs
Merge
ZH
ZH
ZH
NI
NI
NI
NI
Hoechst
H.
NSs
Abl2
Hoechst
F-actin
Merge
NI 8h
ZH 8h
ZH 24h

Figure 4

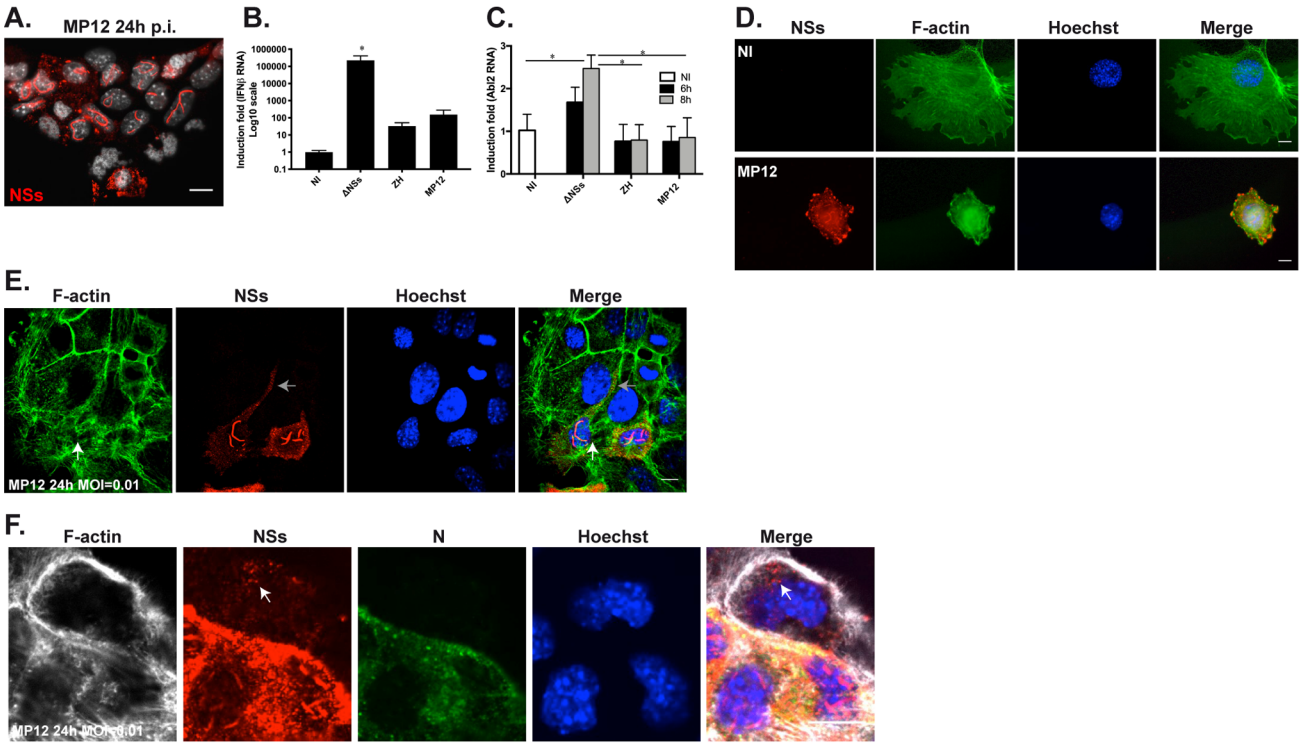
A.
MP12 24h p.i.
NSs
B.
Induction fold (IFNβ RNA)
Log10 scale
1000000
100000
10000
1000
100
10
1
0.1
NI
ΔNSs
ZH
MP12
C.
Induction fold (Abl2 RNA)
3
2
1
0
NI
6h
8h
NI
ΔNSs
ZH
MP12
D.
NSs
F-actin
Hoechst
Merge
NI
MP12
E.
F-actin
NSs
Hoechst
Merge
MP12 24h MOI=0.01
F.
F-actin
NSs
N
Hoechst
Merge
MP12 24h MOI=0.01

Figure 5

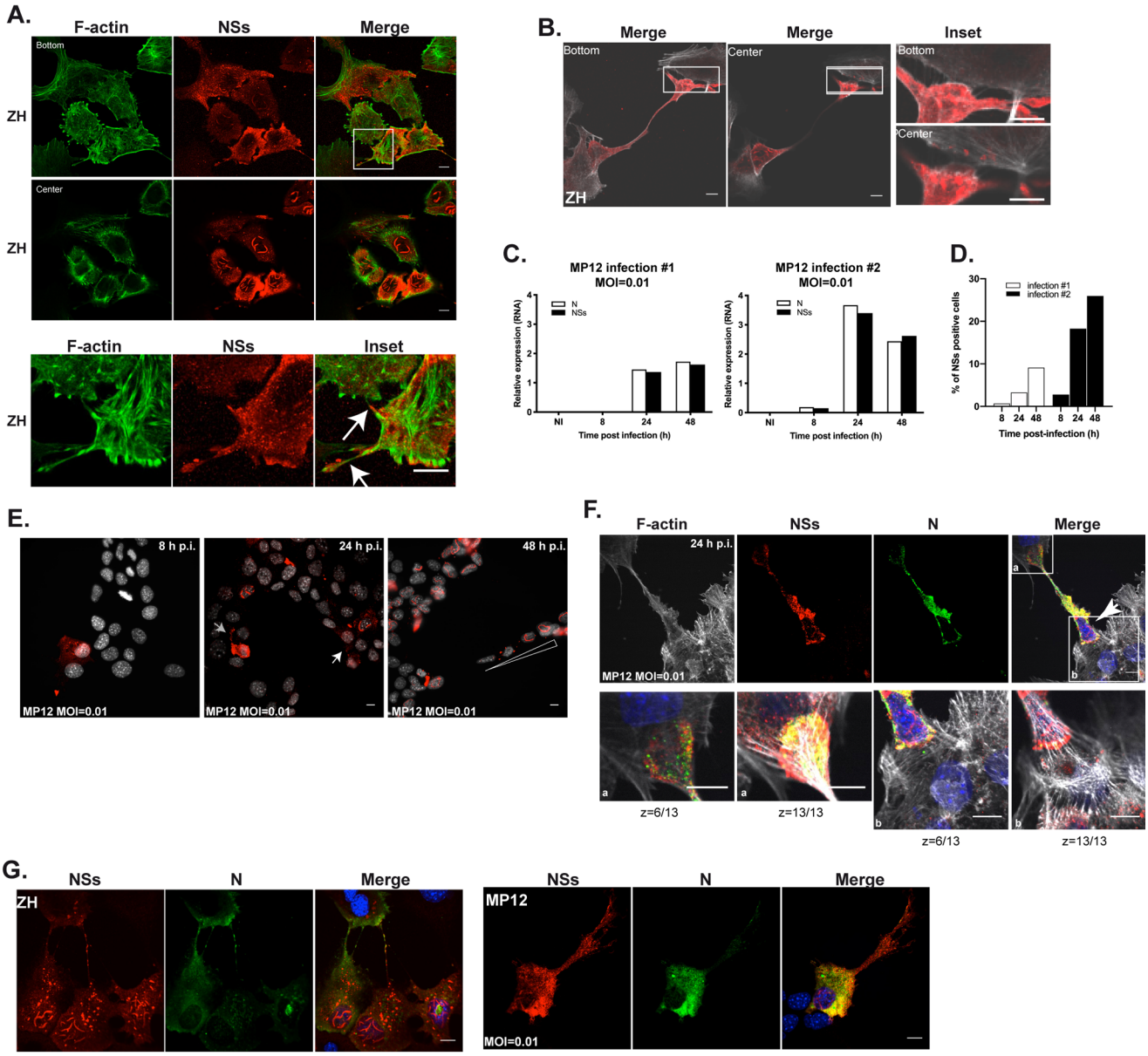
A.
F-actin
NSs
Merge
Bottom
ZH
Center
ZH
F-actin
NSs
Inset
ZH
B.
Merge
Merge
Inset
Bottom
Center
Bottom
Center
ZH
C.
MP12 infection #1
MOI=0.01
MP12 infection #2
MOI=0.01
N
NSs
Relative expression (RNA)
NI
8
24
48
Time post infection (h)
D.
infection #1
infection #2
% of NSs positive cells
8 24 48 8 24 48
Time post-infection (h)
E.
8 h p.i.
24 h p.i.
48 h p.i.
MP12 MOI=0.01
MP12 MOI=0.01
MP12 MOI=0.01
F.
F-actin
NSs
N
Merge
24 h p.i.
MP12 MOI=0.01
a
b
z=6/13
z=13/13
z=6/13
z=13/13
G.
NSs
N
Merge
ZH
NSs
N
Merge
MP12
MOI=0.01

Figure 6

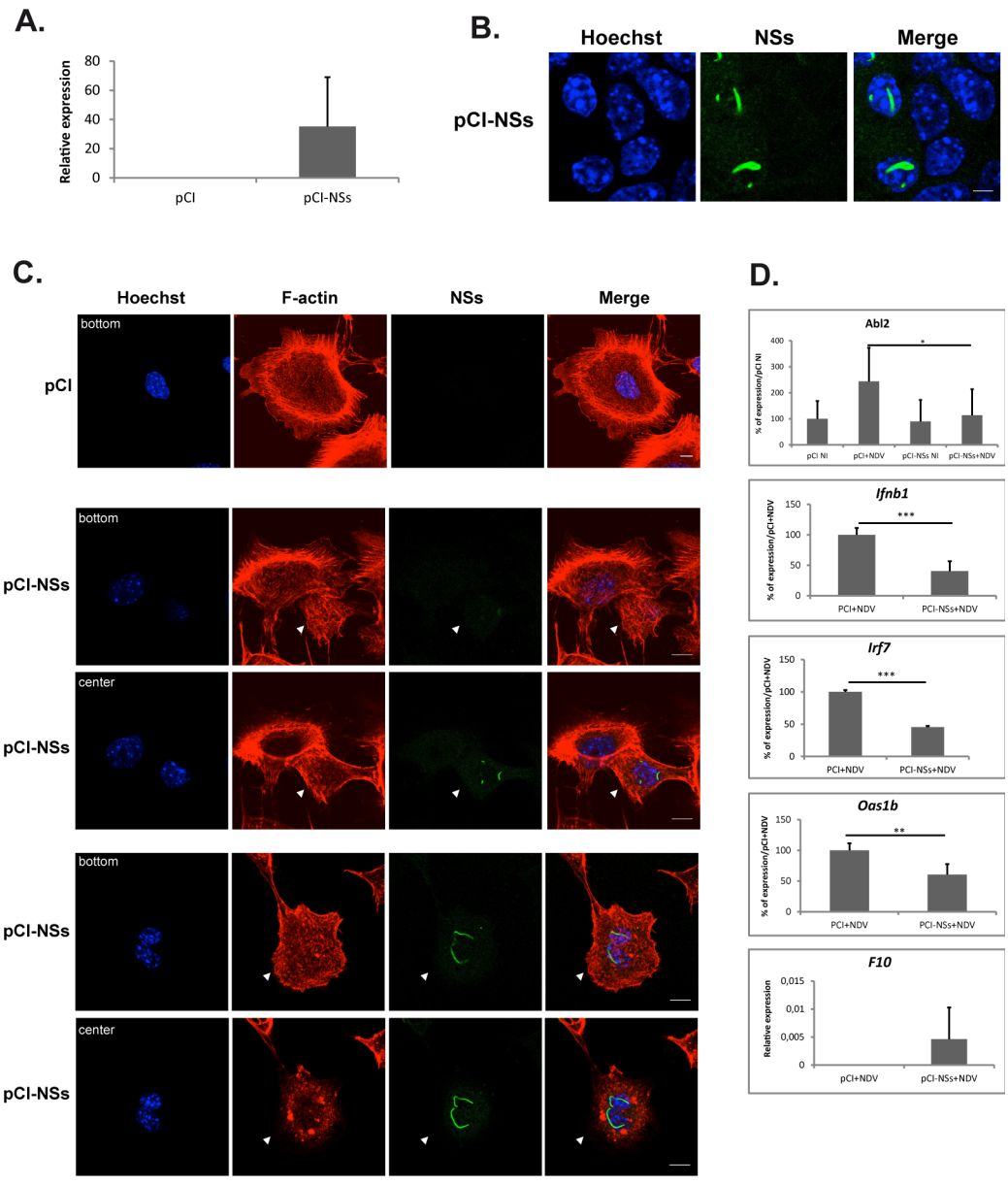
A.
Relative expression
80
60
40
20
0
pCI
pCI-NSs
B.
Hoechst
NSs
Merge
pCI-NSs
C.
Hoechst
F-actin
NSs
Merge
pCI
bottom
pCI-NSs
bottom
pCI-NSs
center
pCI-NSs
bottom
pCI-NSs
center
D.
Abl2
% of expression/pCI NI
400
300
200
100
0
pCI NI
pCI+NDV
pCI-NSs NI
pCI-NSs+NDV
*
Ifnb1
% of expression/pCI+NDV
150
100
50
0
PCI+NDV
PCI-NSs+NDV
***
Irf7
% of expression/pCI+NDV
150
100
50
0
PCI+NDV
PCI-NSs+NDV
***
Oas1b
% of expression/pCI+NDV
150
100
50
0
PCI+NDV
PCI-NSs+NDV
**
F10
Relative expression
0,015
0,01
0,005
0
pCI+NDV
pCI-NSs+NDV

Figure 7